

Efficient Imputation for Patch-based Missing Single-cell Data via Cluster-regularized Optimal Transport

Yuyu Liu¹, Jiannan Yang¹, Ziyang Yu², Weishen Pan³, Fei Wang³, and Tengfei Ma¹

¹ Department of Computer Science, Stony Brook University, Stony Brook, NY, USA

² Department of Computer Science, Emory University, Atlanta, GA, USA

³ Department of Computer Science, Cornell University, Ithaca, NY, USA

Abstract. Missing data in single-cell sequencing datasets poses significant challenges for extracting meaningful biological insights. However, existing imputation approaches, which often assume uniformity and data completeness, struggle to address cases with large patches of missing data. In this paper, we present **CROT** (Cluster-Regularized Optimal Transport), an optimal transport-based imputation algorithm designed to handle patch-based missing data in tabular formats. Our approach effectively captures the underlying data structure in the presence of significant missingness. Notably, it achieves superior imputation accuracy while significantly reducing runtime, demonstrating its scalability and efficiency for large-scale datasets. This work introduces a robust solution for imputation in heterogeneous, high-dimensional datasets with structured data absence, addressing critical challenges in both biological and clinical data analysis. Our code is available at Anomalous G ithub.

Keywords: Optimal transport, Single-cell sequencing analysis, Patchwork learning, Data imputation

1 Introduction

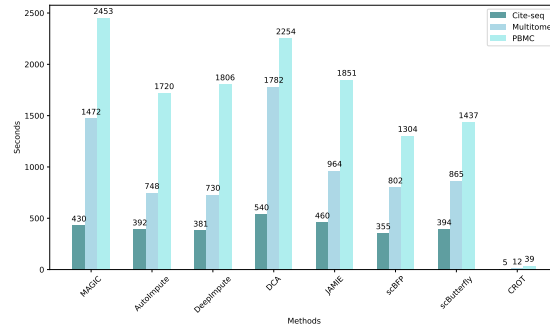


Fig. 1. Runtime comparison on three datasets. Calculated as the total time of model initialization, model training, and inference on the dataset (if the method is model-dependent), or the total time of iterative interpolation on the target dataset (if the method is not model-dependent). The final results are truncated to integers.

Single-cell sequencing technologies have revolutionized our ability to profile gene expression at the resolution of individual cells, uncovering diverse cell types and states within complex tissues. However, these datasets are notoriously sparse, containing many zero values due to both biological reasons (true lack of gene expression) and technical limitations (insufficient mRNA capture or sequencing depth). Such “dropout” events can severely hinder downstream analysis and diminish the power of single-cell

studies if left unaddressed [7]. In practice, this means important biological insights—like identifying rare cell subpopulations or accurately mapping developmental trajectories—may be obscured by noise. Imputation of missing or zeroed-out values is therefore critical to recover meaningful biological signals and enable robust analysis of cellular heterogeneity.

A growing number of methods have been developed to tackle dropout imputation in single-cell RNA-seq data. Early approaches such as MAGIC[16] diffuse information across similar cells to smooth out zeros, while scImpute [10] fits mixture models to distinguish true zero expression from technical dropouts. Bayesian methods like SAVER [6] borrow information across genes to infer likely expression values. More recently, deep learning techniques have emerged: multi-modal frameworks like JAMIE [4] use variational autoencoders to impute one modality from another. However, most existing methods make strong assumptions about data completeness or uniform missingness and tend to borrow information only from local similarities (neighboring cells or genes). This can lead to over-smoothing of the data (blurring true biological distinctions) and loss of natural cell-to-cell variability. Crucially, many methods struggle when faced with patch-based missing data—the extreme scenario where entire blocks of features (such as whole gene sets or entire assay modalities) are absent for a subset of the dataset. Such situations can arise, for example, if a technical failure causes all cells from one experimental batch to lack a particular measurement (e.g., all ADT protein tags missing in one CITE-seq batch, or all gene expression values missing for a condition in a multi-omic experiment). Traditional dropout-focused algorithms are not equipped to handle these large, structured absences, since they assume each feature is at least partially observed across the dataset.

To address these challenges, Cluster-Regularized Optimal Transport (CROT) is proposed. Our approach is motivated by two key insights: (1) When one subset of data is missing entire features, a powerful way to infer those missing values is to align the distribution of the incomplete data with that of a related complete dataset. (2) Simply aligning global distributions might ignore the internal structure that is crucial in biology – specifically, the presence of distinct cell subpopulations or clusters (e.g. cell types, states). Therefore, CROT augments the OT mapping with a cluster regularization term that preserves the similarity of cluster centroids (representative cell-type expression profiles) between the complete and incomplete data. By explicitly enforcing that the imputed data recapitulates the same cell-type structure as the reference data, we maintain inter-cell-type specificity and avoid collapsing distinct cell identities. The biological relevance of this strategy is clear. For example, if T cells and B cells form separate clusters in a fully observed dataset, our method strives to ensure that after imputation, T cells and B cells in the previously incomplete dataset are still well-separated and each cluster’s prototype expression remains accurate. Our contributions can be summarized as follows:

- We propose a cluster-regularized optimal transport imputation method that effectively captures the intricate relations within single-cell data batches, demonstrating high accuracy in imputing dropout events.
- Our method achieves not only superior imputation performance but also demonstrates fast convergence, making it highly efficient for large-scale single-cell datasets.
- We conduct extensive experiments on multiple single-cell datasets to evaluate our approach under various missing data scenarios. Our results indicate that CROT outperforms state-of-the-art imputation methods in both accuracy and computational efficiency.

2 Related Work

In this section, we review related works, including existing OT-based and non-OT-based imputation methods for single-cell and general data.

2.1 Single-cell Sequencing Data Imputation

Single-cell sequencing data frequently encounters dropout events, leading to numerous zeros that obstruct downstream analyses. To mitigate this issue, a variety of computational and statistical methods

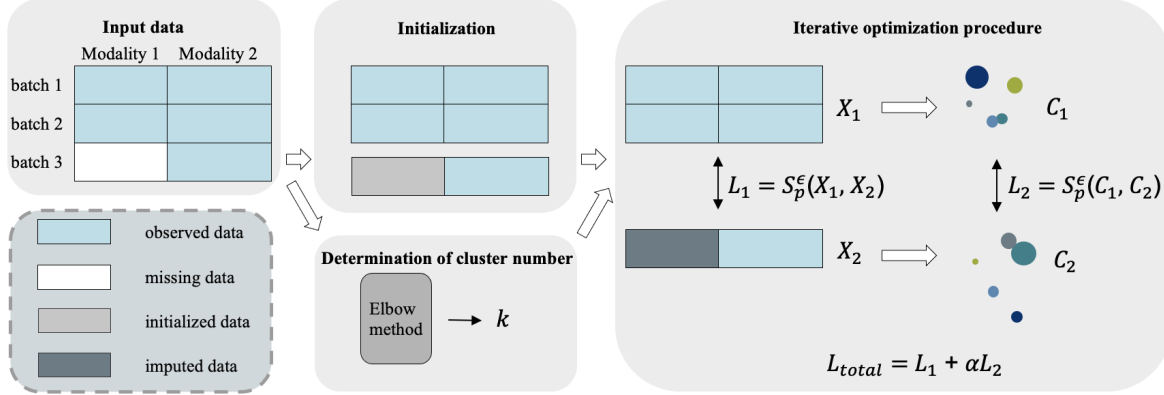


Fig. 2. An illustration of our framework. Assume that all modality 1 data from batch 3 is missing (where “modality” may vary by dataset). The process begins by initializing the missing data and using observed data from batches 1 and 2 to determine an optimal number of clusters. The following iterative optimization procedure is then applied. In each iteration, clustering with k clusters is performed to assign a class label to each row in X_1 and X_2 , respectively. Next, centroids C_1 and C_2 are calculated by averaging the rows belonging to each class. Subsequently, the Sinkhorn divergence between (X_1, X_2) and (C_1, C_2) is computed to form the total loss. This procedure continues until the total loss converges.

have been proposed. Notable approaches include MAGIC [16], which utilizes data diffusion to smooth out dropouts; scImpute [10], which distinguishes true zeros from dropouts through a mixture model; and SAVER [6], which applies a Bayesian approach to impute missing values while considering gene expression variability. Additionally, scGNN [17] employs graph neural networks to account for cellular neighborhood relationships, while ALRA [11] utilizes adaptive low-rank autoregressive models to capture temporal dependencies in gene expression profiles. Although these methods have demonstrated efficacy in enhancing clustering, visualization, and gene expression analysis, they often struggle under conditions of extensive missing data and may not fully leverage the inherent structural relationships within the data.

2.2 Optimal Transport in Data Imputation

Optimal transport (OT) has been widely employed for data imputation across various domains. For instance, [13] proposed an OT-based loss function for imputing missing values, demonstrating its efficacy across multiple datasets. Similarly, [18] introduced Git, a generative imputation model that leverages OT for multi-view data imputation, achieving notable performance improvements in multi-view scenarios. In the realm of single-cell multi-modal data, [1] developed CMOT (Cross-Modality Optimal Transport), which utilizes OT to align cells across different modalities and infer missing data. Additionally, [8] presented the GENOT framework, which employs entropic OT to predict cellular responses and translate across data modalities, thereby addressing complex data integration challenges. Despite their successes, these methods often overlook the critical link between data integrity and downstream tasks, such as cell-type clustering, that depend on accurate and biologically meaningful imputation.

2.3 Patchwork Learning

In recent work, Patchwork Learning (PL) has emerged as a compelling approach to handling heterogeneous data sources, particularly in healthcare contexts where data is distributed across multiple sites with varying modalities. Rajendran et al. [14] introduce PL as a framework that enables the integration of disparate datasets, even when certain sites lack complete modalities, by leveraging bridging modalities or shared features across sites. This approach aligns closely with our missing data patch

setting, where partial features from one or more sites are unavailable. By addressing the challenge of incomplete data across distributed networks, PL facilitates more robust and generalizable machine learning models, capable of imputing missing data and ensuring data privacy.

3 Preliminary

Optimal transport (OT) theory provides a powerful tool for comparing probability distributions by solving the problem of moving mass between distributions at minimal cost. Given two probability distributions μ and ν with supports $\Omega, \Omega^* \subset \mathcal{X}$, where \mathcal{X} is a Polish space (e.g. \mathbb{R}^n), the Wasserstein distance of order p is defined as:

$$W_p(\mu, \nu) := \inf_{\gamma \in \Pi(\mu, \nu)} \left(\int_{\mathcal{X} \times \mathcal{X}} c(x, y)^p d\gamma(x, y) \right)^{\frac{1}{p}} \quad (1)$$

where $c(\cdot, \cdot) : \mathcal{X} \times \mathcal{X} \rightarrow \mathbb{R}_{\geq 0}$ is the cost function of two points in \mathcal{X} , and $\Pi(\mu, \nu)$ denotes the set of all joint distributions (or couplings) γ with marginals μ and ν . This distance, though geometrically meaningful, is computationally expensive, particularly in high dimensions.

To alleviate this, entropic regularization introduces an entropy term into the optimization, modifying the objective as follows:

$$W_p^\epsilon(\mu, \nu) := \inf_{\gamma} \left(\int c(x, y)^p d\gamma + \epsilon \text{KL}(\gamma \parallel \mu \otimes \nu) \right)^{\frac{1}{p}} \quad (2)$$

where $\text{KL}(\cdot \parallel \cdot)$ is the Kullback-Leibler divergence between γ and the independent coupling $\mu \otimes \nu$, and $\epsilon > 0$ controls the strength of the regularization. The added entropy facilitates faster convergence via iterative algorithms, notably the Sinkhorn-Knopp algorithm.

The resulting metric, known as the Sinkhorn divergence, approximates the original Wasserstein distance while offering significant computational speed-ups:

$$S_p^\epsilon(\mu, \nu) := W_p^\epsilon(\mu, \nu) - \frac{1}{2} (W_p^\epsilon(\mu, \mu) + W_p^\epsilon(\nu, \nu)) \quad (3)$$

This divergence retains the essential properties of the Wasserstein distance but benefits from the computational efficiency introduced by the regularization, making it particularly well-suited for large-scale applications where OT-based techniques are needed to compare distributions.

4 Methodology

In this section, we present the details of CROT for imputing missing values in tabular data and analyze its computational complexity. Our framework is shown in Figure 2.

4.1 Cluster-regularized Optimal Transport

To impute missing data, we first consider information transfer at the data level. Let X_1 and X_2 be two sets of tabular data, where $X_1 \in \mathbb{R}^{m_1 \times n}$ is the set of m_1 observed data, and $X_2 \in \mathbb{R}^{m_2 \times n}$ is the set containing missing values to be imputed. We can simplify the Wasserstein distance between these two sets of discrete samples X_1 and X_2 from eq. 1 to

$$W_p(X_1, X_2) = \inf_{\gamma} \left(\sum_{i,j} c(X_1[i, :], X_2[j, :])^p \gamma_{ij} \right)^{\frac{1}{p}} \quad (4)$$

Algorithm 1 Cluster-regularized Optimal Transport**Input:** $X_1 \in \mathbb{R}^{m_1 \times n}$, $X_2 \in \mathbb{R}^{m_2 \times n}$, $\epsilon, T, \alpha, l > 0$, missing columns S in X_2 , number of clusters k **Output:** Completed data \hat{X}_2 **Initialization:**

```

1: for  $j \in S$  do
2:   for  $i = 1, \dots, m_2$  do
3:      $\hat{X}_2[i, j] \leftarrow \text{mean}(X_1[:, j]) + \epsilon_{ij}$ ,
       where  $\epsilon_{ij} \sim \mathcal{N}(0, 1)$ 
4:   end for
5: end for

```

Optimization:

```

1: for  $t = 1, \dots, T$  do
2:   Sample two sets  $K, L$  of  $l$  indices from  $X_1$  and  $\hat{X}_2$ , respectively
3:    $(C_{1K}, \hat{C}_{2L}) \leftarrow \text{Clustering}_k(X_{1K}, \hat{X}_{2L})$ 
4:    $\mathcal{L} \leftarrow S_p^\epsilon(X_{1K}, \hat{X}_{2L}) + \alpha S_p^\epsilon(C_{1K}, \hat{C}_{2L})$ 
5:    $\hat{X}_{2L}^{(imp)} \leftarrow \hat{X}_{2L}^{(imp)} - \text{Adam}(\nabla_{\hat{X}_{2L}^{(imp)}} \mathcal{L})$ 
6: end for

```

where we use the Euclidean L_2 distance as the cost function c , and the marginals of transference plan γ are uniform distributions.

Consequently, the discrete version of Sinkhorn divergence between X_1 and X_2 , denoted by $S_p^\epsilon(X_1, X_2)$, constitutes the main part of the total loss function. Minimizing this distance maps features in X_1 to features in X_2 , thereby imputing missing values in X_2 .

However, this method ignores the consistency of clustering structures between different sets of data. For X_1 and X_2 , we expect not only the alignment between the data sample distributions but also the alignment between cluster distributions. For example, for different sets of single cell sequencing data in the same domain, we may want their cell-type prototypes also to remain similar. Therefore, we incorporate cluster regularization by computing the Wasserstein distance between the cluster centers of the complete data and the missing data. The cluster centers are obtained from the average of entries within each class, calculated along the rows of X_1 and X_2 .

In order to obtain effective clusters, we use the Elbow method to heuristically determine the optimal number k of clusters in X_1 . Based on the similarity assumption of X_1 and X_2 , we regard it as an approximation of the number of clusters in X_2 . At each iteration, we perform clustering with k clusters on X_1 and X_2 , where the cluster centers are given by:

$$c_s(X_1) := \frac{1}{|C_{1,s}|} \sum_{i \in C_s} X_1[i, :] \\ c_t(X_2) := \frac{1}{|C_{2,t}|} \sum_{j \in C_{2,t}} X_2[j, :]$$

where $C_{1,s}$ is the set of indices assigned to cluster s in X_1 , and similar for $C_{2,t}$. These cluster centers are then used to compute the Wasserstein distance between the complete data (from X_1) and the imputed data (from X_2). Let the two sets of cluster centers computed from X_1, X_2 be \mathcal{C}_1 and \mathcal{C}_2 , respectively. Finally, we define the cluster-regularized OT loss as follows:

$$L_{\text{CROT}}(X_1, X_2) = S_p^\epsilon(X_1, X_2) + \alpha S_p^\epsilon(\mathcal{C}_1, \mathcal{C}_2) \quad (5)$$

The second term is a regularization term that encourages the cluster centers of the imputed data to align closely with the complete data. The constant $\alpha > 0$ controls the trade-off between these two objectives. Since the overall distribution of the two data matrices is relatively similar, the relationship between each cluster is also similar, resulting in no order of magnitude difference between

calculating the Sinkhorn distance between the entire data and using only the center points. Therefore, no additional adjustments are needed to α . Finally, we illustrate the overall optimization strategy of CROT in Algorithm 1.

4.2 Complexity Analysis

The complexity analysis of the algorithm is divided into the following two main phases:

Phase 1: Initialization During the initialization process, the algorithm iterates over each missing column indexed by j in S and each row i in X_2 , where $X_2[i, j]$ is updated based on the mean of corresponding entries in X_1 . Computing this mean requires $O(m_1)$ time, where m_1 is the number of rows in X_1 . Given that there are $|S|$ missing columns in X_2 , the time complexity for initialization is $O(|S| \cdot m_1)$. Meanwhile, The Elbow method is used to determine the optimal number of clusters k for a k-means clustering algorithm using X_1 . It involves running k-means K with different values of k and calculating the within-cluster sum of squares (WCSS) for each k . The time complexity of the k-means algorithm is costs $O(l \cdot k \cdot i)$, where i is a constant that represents the number of iterations; and running for K times results in $O(K \cdot i \cdot m_1 \cdot k \cdot n)$, which could be simplified to $O(m_1 \cdot n)$ since K is typically a small number compared to m_1 . Therefore, the total time complexity of phase 1 is $O(m_1 \cdot n)$

Phase 2: Iterative Optimization The main loop runs for T iterations. In each iteration, two sets of l indices are sampled from matrices X_1 and X_2 , costing $O(l)$ time. For each sampled set with shape $l \times n$, k-means algorithm is applied to assign a label for each row, costing $O(l \cdot k \cdot i)$. The Sinkhorn algorithm has a time complexity of $O(T \cdot l^2)$, where T is the number of iterations, dominated by operations on the $l \times l$ transport matrix. The Adam optimizer adds a minor overhead of $O(l \cdot n)$ for the parameter update step. However, since l^2 dominates, the overall time complexity per iteration remains $O(T \cdot l^2)$.

Table 1. Results of missing data recovery on Citeseq, Multiome, and PBMC. Each value is reported as mean \pm standard deviation over five random batch pairs.

Dataset	Citeseq			Multiome			PBMC			
	Metrics	PCC	MAE	RMSE	PCC	MAE	RMSE	PCC	MAE	RMSE
RAW		nan	3.99 \pm 0.03	4.10 \pm 0.06	nan	2.07 \pm 0.10	2.18 \pm 0.07	nan	1.30 \pm 0.05	1.44 \pm 0.09
MAGIC		0.72 \pm 0.11	1.03 \pm 0.06	1.19 \pm 0.04	0.17 \pm 0.08	1.08 \pm 0.05	1.19 \pm 0.07	0.62 \pm 0.04	0.92 \pm 0.09	1.04 \pm 0.15
AutoImpute		0.70 \pm 0.12	0.72 \pm 0.03	0.62 \pm 0.03	0.09 \pm 0.14	4.70 \pm 0.21	6.85 \pm 0.33	0.52 \pm 0.02	0.93 \pm 0.04	0.99 \pm 0.05
DeepImpute		0.54 \pm 0.12	7.61 \pm 0.13	12.05 \pm 0.54	0.12 \pm 0.02	2.36 \pm 0.13	3.70 \pm 0.19	0.50 \pm 0.02	1.53 \pm 0.07	1.97 \pm 0.09
DCA		0.60 \pm 0.01	1.08 \pm 0.09	1.29 \pm 0.06	0.09 \pm 0.09	2.44 \pm 0.10	2.94 \pm 0.12	0.53 \pm 0.12	1.89 \pm 0.08	2.28 \pm 0.10
JAMIE		0.69 \pm 0.02	1.09 \pm 0.09	1.27 \pm 0.06	0.21 \pm 0.03	1.80 \pm 0.09	1.97 \pm 0.09	0.58 \pm 0.09	1.23 \pm 0.06	1.40 \pm 0.07
scBFP		0.58 \pm 0.02	0.70 \pm 0.13	0.99 \pm 0.04	0.06 \pm 0.04	1.45 \pm 0.06	1.62 \pm 0.06	0.56 \pm 0.04	2.03 \pm 0.09	2.30 \pm 0.10
scButterfly		0.71 \pm 0.02	0.94 \pm 0.06	1.25 \pm 0.05	0.15 \pm 0.02	1.69 \pm 0.07	1.88 \pm 0.09	0.59 \pm 0.05	0.93 \pm 0.05	1.17 \pm 0.07
CROT		0.76 \pm 0.04	0.47 \pm 0.07	0.99 \pm 0.03	0.22 \pm 0.09	0.59 \pm 0.03	1.18 \pm 0.03	0.64 \pm 0.11	0.75 \pm 0.03	0.88 \pm 0.03

Combining both phases, the overall time complexity of the algorithm is $O(m_1 \cdot n + T \cdot l^2)$. Since l is a small constant with respect to the number of sampled lines, the overall time complexity increases linearly with the size of X_1 , making the imputation process fast and efficient. The space complexity is dominated by storing matrices X_1 and X_2 , resulting in $O(m_1 \cdot n + m_2 \cdot n)$.

5 Experiment

In this section, we evaluate the effectiveness of the proposed method. We first measure the similarity between the original and the imputed data, followed by the cell-type task on several widely used datasets. In addition, we demonstrate the lightweightness of the proposed approach by conducting several imputing efficiency comparison studies.

5.1 Dataset and Experiment Settings

To validate the effectiveness of our method on real-world data, we conduct experiments on three widely used single-cell sequencing datasets. The BMMC-citeseq dataset [12] contains RNA and protein expression data from bone marrow mononuclear cells obtained using CITE-seq technology, allowing multi-omics analysis. The BMMC-multiome dataset includes paired measurements of chromatin accessibility and gene expression from BMMC, providing insight into gene regulation at a single-cell level. The PBMC dataset⁴ offers gene expression profiling of peripheral blood mononuclear cells, which is commonly used for investigating immune cell diversity and function. The detailed data preprocessing process can be found in Supplementary Materials Section A.1.

To evaluate the robustness and generalizability of CROT under realistic multimodal missingness, we simulate patch-based modality dropout following the multi-batch structure of each dataset. Specifically, for each dataset (CITE-seq, Multiome, and PBMC), we randomly select multiple independent subsets (“batches”) that represent distinct experimental replicates or donor groups. In each trial, one batch is treated as complete (all modalities available) and another as incomplete (one modality entirely masked, e.g., all ADT values or all RNA counts set as missing). The complete batch serves as the reference domain X_1 , while the incomplete batch is the target domain X_2 to be imputed using our CROT algorithm. To account for variability, we repeat this procedure across five random pairs of batches and report the mean and standard deviation of all metrics. During imputation, we initialize missing modality features in X_2 using column means from X_1 , then iteratively refine them via our cluster-regularized optimal transport objective until convergence. This produces a completed matrix X_2 where the missing modality is reconstructed by aligning both the global feature distributions and the cluster-level centroids between X_1 and X_2 .

In our experiments, we empirically set the regularization parameter $\alpha = 1$, as discussed in Section 4.1.

5.2 Evaluation Metrics

Numerical Recovery We assess the recovery performance of CROT using Root Mean Square Error (RMSE), Mean Absolute Error (MAE), and Pearson Correlation Coefficient (PCC). RMSE and MAE quantify the numerical discrepancies between the imputed data and the true expression values, where lower RMSE and MAE values signify more accurate imputation. PCC, on the other hand, is a similarity measurement that evaluates the correlation between imputed and true expression data. A PCC value closer to 1 indicates a higher degree of similarity, reflecting the effectiveness of the imputation method employed in this study

Clustering Representation To evaluate structural preservation, we employ clustering metrics such as Adjusted Rand Index (ARI), Normalized Mutual Information (NMI), and Purity. These metrics assess the extent to which the imputation retains meaningful clusters by comparing the imputed data to the ground-truth clusters. For qualitative analysis, we use Uniform Manifold Approximation and Projection (UMAP) for dimensionality reduction, allowing visual comparison of the original and imputed data in a lower-dimensional space.

Efficiency Additionally, we measure running time to evaluate computational efficiency, providing insight into the scalability of the method.

⁴ <https://www.10xgenomics.com/datasets>

Table 2. Results of cell type clustering on Citeseq, Multiome, and PBMC. Each value is reported as mean \pm standard deviation over five random batch pairs.

Dataset	Citeseq			Multiome			PBMC			
	Metrics	ARI	NMI	PURITY	ARI	NMI	PURITY	ARI	NMI	PURITY
RAW		0.65 \pm 0.02	0.67 \pm 0.03	0.77 \pm 0.02	0.49 \pm 0.02	0.62 \pm 0.03	0.67 \pm 0.03	0.53 \pm 0.06	0.73 \pm 0.04	0.95 \pm 0.03
AutoImpute		0.80 \pm 0.03	0.81 \pm 0.12	0.89 \pm 0.02	0.13 \pm 0.02	0.33 \pm 0.03	0.34 \pm 0.07	0.34 \pm 0.02	0.44 \pm 0.03	0.90 \pm 0.02
DeepImpute		0.53 \pm 0.02	0.67 \pm 0.03	0.82 \pm 0.03	0.45 \pm 0.02	0.58 \pm 0.03	0.60 \pm 0.03	0.38 \pm 0.02	0.51 \pm 0.03	0.84 \pm 0.02
DCA		0.68 \pm 0.02	0.72 \pm 0.03	0.78 \pm 0.03	0.16 \pm 0.02	0.19 \pm 0.03	0.62 \pm 0.03	0.38 \pm 0.02	0.49 \pm 0.03	0.88 \pm 0.02
JAMIE		0.72 \pm 0.08	0.71 \pm 0.07	0.78 \pm 0.09	0.44 \pm 0.11	0.61 \pm 0.08	0.62 \pm 0.07	0.40 \pm 0.06	0.69 \pm 0.03	0.89 \pm 0.07
scBFP		0.22 \pm 0.07	0.57 \pm 0.03	0.84 \pm 0.02	0.10 \pm 0.01	0.37 \pm 0.03	0.50 \pm 0.03	0.13 \pm 0.01	0.72 \pm 0.03	0.92 \pm 0.05
scButterfly		0.69 \pm 0.02	0.72 \pm 0.03	0.81 \pm 0.03	0.36 \pm 0.02	0.53 \pm 0.03	0.63 \pm 0.03	0.21 \pm 0.02	0.50 \pm 0.03	0.88 \pm 0.02
CROT		0.82\pm0.01	0.75\pm0.02	0.93\pm0.03	0.68\pm0.01	0.79\pm0.02	0.70\pm0.02	0.64\pm0.01	0.77\pm0.02	0.96\pm0.01

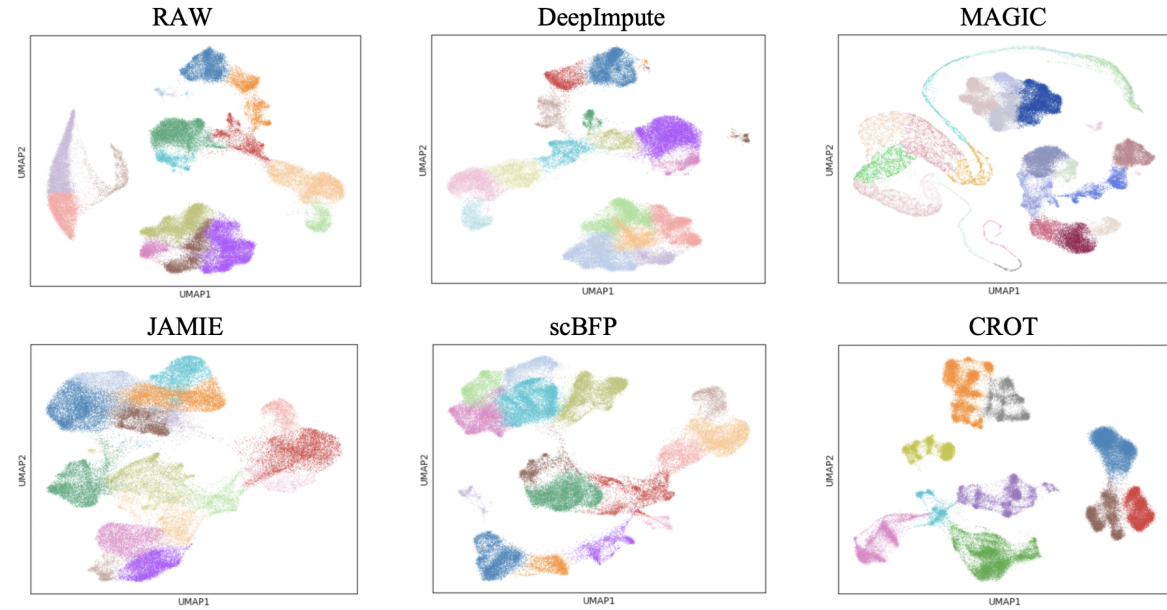


Fig. 3. UMAP visualizations comparing clustering quality across different imputation methods. Better distinct clusters of UMAP plots helps with further analysis of single-cell data, such as the presence of rare cell types or intermediate states between well-defined populations.

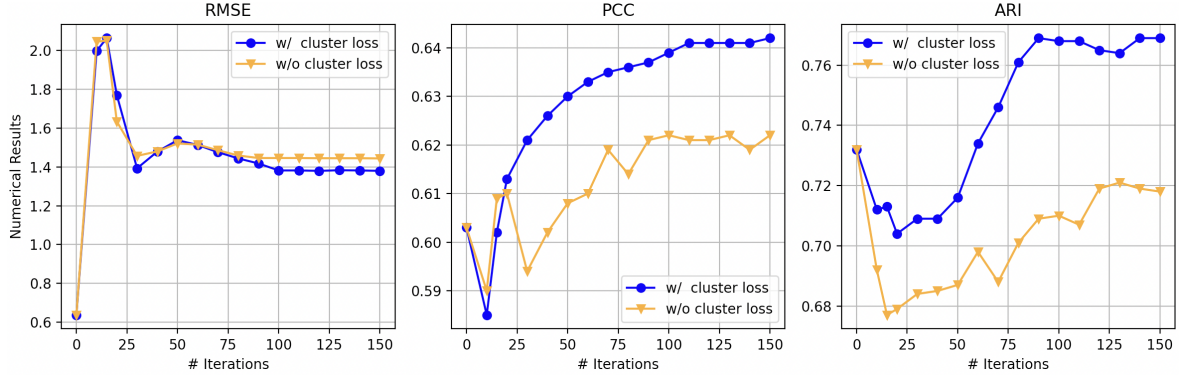


Fig. 4. Numerical value of RMSE, PCC and ARI on one missing setting of Citeseq during iterative imputation process.

5.3 Baselines

We evaluate the performance of our method against several state-of-the-art models for single-cell sequencing, focusing on tasks such as data recovery and clustering. The selected single-cell imputation baselines include MAGIC [16], AutoImpute [15], DeepImpute [2], JAMIE [4], scBFP [9], DCA [5] and scButterfly [3]. Detailed descriptions of these methods are available in Section A.2 of Supplementary Materials.

In addition to these baselines, we also assessed clustering performance on raw data without imputation (denoted as RAW) to demonstrate the necessity of the data imputation.

5.4 Missing Data Recovering

To test the authenticity of the data estimated by our method, we compared the correlation and similarity between the imputed data and the real data. The experimental results on single-cell data are displayed in Table 1. Our method achieves the highest PCC and lowest MAE values across all datasets, indicating superior imputation accuracy compared to other methods.

5.5 Clustering Analysis

Cell Type and Phenotype Clustering Identifying cell types and phenotypes from diverse populations of single cells and patients, respectively, relies on effective clustering techniques, which group entities based on similarities, such as gene expression or clinical features. However, the presence of missing data can interfere with clustering performance. Thus we first apply all imputation methods to get the imputed data and then evaluate the clustering effectiveness using Leiden algorithm. The results in Table 2 show that raw data (without imputation) clustering is consistently inferior to imputed data clustering, implying the importance and necessity of imputation. Among the imputation methods, CROT achieves the best performance in cell type clustering on Citeseq, Multiome, and PBMC datasets, with the highest Adjusted Rand Index (ARI) and Purity, such as 0.815 and 0.929 on Citeseq, and 0.643 and 0.958 on PBMC.

Visualization of Imputed Data In addition, we also provide the UMAP plots of imputed data by several methods on Multiome data in Figure 5. Compared with the graph for raw data, where the clusters appear less distinct and more dispersed, all methods show gradual improvements in cluster separation. Notably, our method demonstrates significantly improved clustering with more distinct clusters than others, indicating that our imputation method better preserves biological heterogeneity and enhances the data's underlying structure. Therefore, our approach more effectively captures the relationships between cells, resulting in more biologically meaningful clusters.

5.6 Computational Efficiency

We compared the training and imputation times of our method against various benchmark methods across four datasets, with results presented in Figure 1. All experiments were performed on a single RTX 4090 GPU. As shown in the figure, our method demonstrates a significantly lower runtime compared to other methods, requiring only 5, 12, and 39 seconds for the Cite-seq, Multiome, and PBMC datasets, respectively. On average, our method's runtime constitutes only 1.12%, 1.29%, and 2.21% of the average runtime of the comparison methods on these three datasets.

5.7 Ablation Study

Effectiveness of Clustering Module We performed an ablation study to assess the individual contributions of the two loss components in our proposed method, with results presented in Table 3. The findings reveal that optimizing solely for similarity among observed entries already provides strong numerical recovery, but the combination of both losses yields the best overall results, underscoring the effectiveness of incorporating clustering regularization into the imputation process.

Table 3. Ablation study on optimization strategy on Citeseq. L_1 and L_2 denote Sinkhorn divergence between data and centroids, respectively. Each value is reported as mean \pm standard deviation over five random batch pairs.

Dataset	Citeseq				
	Metrics	PCC	RMSE	ARI	NMI
CROT (w/o L_2)	0.74 \pm 0.02	1.28 \pm 0.05	0.78 \pm 0.03	0.60 \pm 0.03	
CROT (w/o L_1)	0.71 \pm 0.02	1.18 \pm 0.04	0.77 \pm 0.03	0.70 \pm 0.03	
CROT (full)	0.76 \pm 0.04	0.99 \pm 0.03	0.82 \pm 0.01	0.75 \pm 0.02	

Improvements over Initialization We conduct an ablation study to assess the impact of cluster regularization on our imputation method, as shown in Figure 4. In one Citeseq setting, RMSE, PCC, and ARI metrics initially decline but subsequently improve, ultimately surpassing initial values except for RMSE. This early decline results from the optimal transport algorithm’s initial imputed values, which are distant from the true distribution. As optimization advances, the algorithm refines the transport plan, aligning the imputed data with the underlying structure. The final RMSE remains higher due to mean column value initialization, which, though numerically similar, lacks biological relevance compared to the more biologically meaningful patterns captured later.

6 Conclusion

We introduced Cluster-Regularized Optimal Transport (CROT), a fast and robust imputation framework designed to address patch-based missingness in single-cell sequencing data. By coupling optimal transport with cluster-level regularization, CROT effectively preserves biological structure while ensuring accurate value recovery. Extensive experiments across multiple datasets demonstrate that CROT achieves superior imputation accuracy and clustering consistency with significantly reduced runtime. These results highlight its practicality for large-scale, multimodal single-cell analysis and its potential as a general solution for structured missing data.

Bibliography

- [1] Sayali Anil Alatkar and Daifeng Wang. CMOT: Cross-Modality Optimal Transport for multi-modal inference. *Genome Biology*, 24(1):163, July 2023. ISSN 1474-760X. <https://doi.org/10.1186/s13059-023-02989-8>. URL <https://genomebiology.biomedcentral.com/articles/10.1186/s13059-023-02989-8>.
- [2] Cédric Arisdakessian, Olivier Poirion, Breck Yunits, Xun Zhu, and Lana X. Garmire. DeepImpute: an accurate, fast, and scalable deep neural network method to impute single-cell RNA-seq data. *Genome Biology*, 20:211, October 2019. ISSN 1474-7596. <https://doi.org/10.1186/s13059-019-1837-6>. URL <https://www.ncbi.nlm.nih.gov/pmc/articles/PMC6798445/>.
- [3] Yichuan Cao, Xiamiao Zhao, Songming Tang, Qun Jiang, Sijie Li, Siyu Li, and Shengquan Chen. scButterfly: a versatile single-cell cross-modality translation method via dual-aligned variational autoencoders. *Nature Communications*, 15(1):2973, April 2024. ISSN 2041-1723. <https://doi.org/10.1038/s41467-024-47418-x>. URL <https://www.nature.com/articles/s41467-024-47418-x>.
- [4] Noah Cohen Kalafut, Xiang Huang, and Daifeng Wang. Joint variational autoencoders for multimodal imputation and embedding. *Nature Machine Intelligence*, 5(6):631–642, May 2023. ISSN 2522-5839. <https://doi.org/10.1038/s42256-023-00663-z>. URL <https://www.nature.com/articles/s42256-023-00663-z>.
- [5] Gökçen Eraslan, Lukas M. Simon, Maria Mircea, Nikola S. Mueller, and Fabian J. Theis. Single-cell RNA-seq denoising using a deep count autoencoder. *Nature Communications*, 10(1):390, January 2019. ISSN 2041-1723. <https://doi.org/10.1038/s41467-018-07931-2>. URL <https://www.nature.com/articles/s41467-018-07931-2>.
- [6] Mo Huang, Jingshu Wang, Eduardo Torre, Hannah Dueck, Sydney Shaffer, Roberto Bonasio, John I. Murray, Arjun Raj, Mingyao Li, and Nancy R. Zhang. SAVER: Gene expression recovery for single-cell RNA sequencing. *Nature methods*, 15(7):539–542, July 2018. ISSN 1548-7091. <https://doi.org/10.1038/s41592-018-0033-z>. URL <https://www.ncbi.nlm.nih.gov/pmc/articles/PMC6030502/>.
- [7] Cheng Jia, Yu Hu, Derek Kelly, Junhyong Kim, Mingyao Li, and Nancy R. Zhang. Accounting for technical noise in differential expression analysis of single-cell RNA sequencing data. *Nucleic Acids Research*, 45(19):10978–10988, November 2017. ISSN 0305-1048, 1362-4962. <https://doi.org/10.1093/nar/gkx754>. URL <http://academic.oup.com/nar/article/45/19/10978/4210934>.
- [8] Dominik Klein, Théo Uscidda, Fabian Theis, and Marco Cuturi. Entropic (Gromov) Wasserstein Flow Matching with GENOT, March 2024. URL <http://arxiv.org/abs/2310.09254>. arXiv:2310.09254 [cs, stat].
- [9] Junseok Lee, Sukwon Yun, Yeongmin Kim, Tianlong Chen, Manolis Kellis, and Chanyoung Park. Single-cell RNA sequencing data imputation using bi-level feature propagation. *Briefings in Bioinformatics*, 25(3):bbae209, May 2024. ISSN 1477-4054. <https://doi.org/10.1093/bib/bbae209>. URL <https://doi.org/10.1093/bib/bbae209>.
- [10] Wei Vivian Li and Jingyi Jessica Li. An accurate and robust imputation method scImpute for single-cell RNA-seq data. *Nature Communications*, 9(1):997, March 2018. ISSN 2041-1723. <https://doi.org/10.1038/s41467-018-03405-7>. URL <https://www.nature.com/articles/s41467-018-03405-7>.
- [11] George C. Linderman, Jun Zhao, Manolis Roulis, Piotr Bielecki, Richard A. Flavell, Boaz Nadler, and Yuval Kluger. Zero-preserving imputation of single-cell RNA-seq data. *Nature Communications*, 13(1):192, January 2022. ISSN 2041-1723. <https://doi.org/10.1038/s41467-021-27729-z>. URL <https://www.nature.com/articles/s41467-021-27729-z>. Publisher: Nature Publishing Group.
- [12] Malte D Luecken, Daniel B Burkhardt, Robrecht Cannoodt, Christopher Lance, Aditi Agrawal, Hananeh Aliee, Ann T Chen, Louise Deconinck, Angela M Detweiler, Alejandro Granados, Shelly

Huynh, Laura Isacco, Yang Joon Kim, Dominik Klein, Joaquin Caceres Melgarejo, Maurizio Morri, Michaela Mueller, Norma F Neff, Bastian Rieck, Kaylie Schneider, Scott Steelman, Michael Sterr, Dan J Treacy, Alexander Tong, Alexandra-Chloé Villani, Guilin Wang, Jia Yan, Ce Zhang, Smita Krishnaswamy, Fabian J Theis, and Jonathan M Bloom. A sandbox for prediction and integration of DNA, RNA, and protein data in single cells. *NeurIPS Datasets and Benchmarks Track (Round 2)*, November 2021.

[13] Boris Muzellec, Julie Josse, Claire Boyer, and Marco Cuturi. Missing Data Imputation using Optimal Transport. *ICML*, 2020.

[14] Suraj Rajendran, Weishen Pan, Mert R. Sabuncu, Yong Chen, Jiayu Zhou, and Fei Wang. Patchwork Learning: A Paradigm Towards Integrative Analysis across Diverse Biomedical Data Sources. *Patterns*, 5(2):100913, February 2024. ISSN 26663899. <https://doi.org/10.1016/j.patter.2023.100913>. URL <http://arxiv.org/abs/2305.06217>. arXiv:2305.06217 [cs].

[15] Divyanshu Talwar, Aanchal Mongia, Debarka Sengupta, and Angshul Majumdar. AutoImpute: Autoencoder based imputation of single-cell RNA-seq data. *Scientific Reports*, 8(1):16329, November 2018. ISSN 2045-2322. <https://doi.org/10.1038/s41598-018-34688-x>. URL <https://www.nature.com/articles/s41598-018-34688-x>. Publisher: Nature Publishing Group.

[16] David Van Dijk, Roshan Sharma, Juozas Nainys, Kristina Yim, Pooja Kathail, Ambrose J. Carr, Cassandra Burdziak, Kevin R. Moon, Christine L. Chaffer, Diwakar Pattabiraman, Brian Bierie, Linas Mazutis, Guy Wolf, Smita Krishnaswamy, and Dana Pe'er. Recovering Gene Interactions from Single-Cell Data Using Data Diffusion. *Cell*, 174(3):716–729.e27, July 2018. ISSN 00928674. <https://doi.org/10.1016/j.cell.2018.05.061>. URL <https://linkinghub.elsevier.com/retrieve/pii/S0092867418307244>.

[17] Juexin Wang, Anjun Ma, Yuzhou Chang, Jianting Gong, Yuexu Jiang, Ren Qi, Cankun Wang, Hongjun Fu, Qin Ma, and Dong Xu. scGNN is a novel graph neural network framework for single-cell RNA-Seq analyses. *Nature Communications*, 12(1):1882, March 2021. ISSN 2041-1723. <https://doi.org/10.1038/s41467-021-22197-x>. URL <https://www.nature.com/articles/s41467-021-22197-x>. Publisher: Nature Publishing Group.

[18] Yangyang Wu, Xiaoye Miao, Xinyu Huang, and Jianwei Yin. Jointly Imputing Multi-View Data with Optimal Transport. *AAAI*, 37(4):4747–4755, June 2023. ISSN 2374-3468. <https://doi.org/10.1609/aaai.v37i4.25599>. URL <https://ojs.aaai.org/index.php/AAAI/article/view/25599>. Number: 4.

A Appendices

A.1 Data Preprocessing

BMMC and PBMCs For single-cell sequencing datasets, we followed standard preprocessing steps. Specifically, data were normalized by each omic, log-transformed (\log_{10}), and highly variable genes were selected. We identified 2000 highly variable genes for gene expression and 4000 for chromatin accessibility. For protein expression, all available features were selected.

A.2 Baselines

AutoImpute utilizes autoencoder-based neural networks to handle sparse gene expression matrices by learning the data's inherent distribution and imputing missing values in scRNA-seq data with minimal modifications to silent gene expressions. MAGIC, another method, employs data diffusion techniques to share information across similar cells, thereby mitigating dropout noise and revealing underlying gene-gene relationships. DeepImpute takes advantage of deep neural networks, leveraging dropout layers and loss functions to predict missing values in scRNA-seq data, with a focus on scalability and efficiency. For multimodal imputation, JAMIE uses joint variational autoencoders, integrating data from different modalities by learning shared latent spaces, which can then be used for cross-modal predictions. ScButterfly extends this approach by incorporating dual-aligned variational autoencoders with data augmentation to facilitate cross-modality translation, specifically targeting scenarios with unpaired or noisy multimodal data. scBFP introduces a two-step graph-based feature propagation for scRNA-seq imputation, combining gene-gene and cell-cell relationships to improve data denoising and imputation accuracy.

A.3 Alignment of Observed and Imputed Data

We plotted umap graphs at different stages of interpolation. As shown in the Fig 5, the class separation effect after using cluster loss is slightly better than that without using it. Our effect is not obvious yet, and we expect to further refine the class constraint strategy in the future.

A.4 Evaluation of Global Structure Consistency

This section presents the PAGA similarity heatmap (Fig 6), a quantitative representation of the global connectivity structure among cell clusters derived from the single-cell RNA-seq data. The heatmap highlights the pairwise connectivity strengths between clusters, computed using the PAGA algorithm. Each value represents the normalized connectivity, reflecting the similarity between clusters based on their transcriptional profiles.

We use the PAGA similarity heatmap to evaluate the global structural consistency before and after data imputation. By comparing heatmaps generated from raw (missing) and imputed datasets, we demonstrate how our proposed imputation method restores biologically meaningful cluster relationships.

A.5 Implementation Details

Since our method is relatively simple, it does not require a lot of parameter tuning. We think that increasing the batch size for each sampling may help, but given the resource constraints, our current choice (batch_size = 3000) has performed well enough.

We follow the suggested hyperparameter settings by the authors:

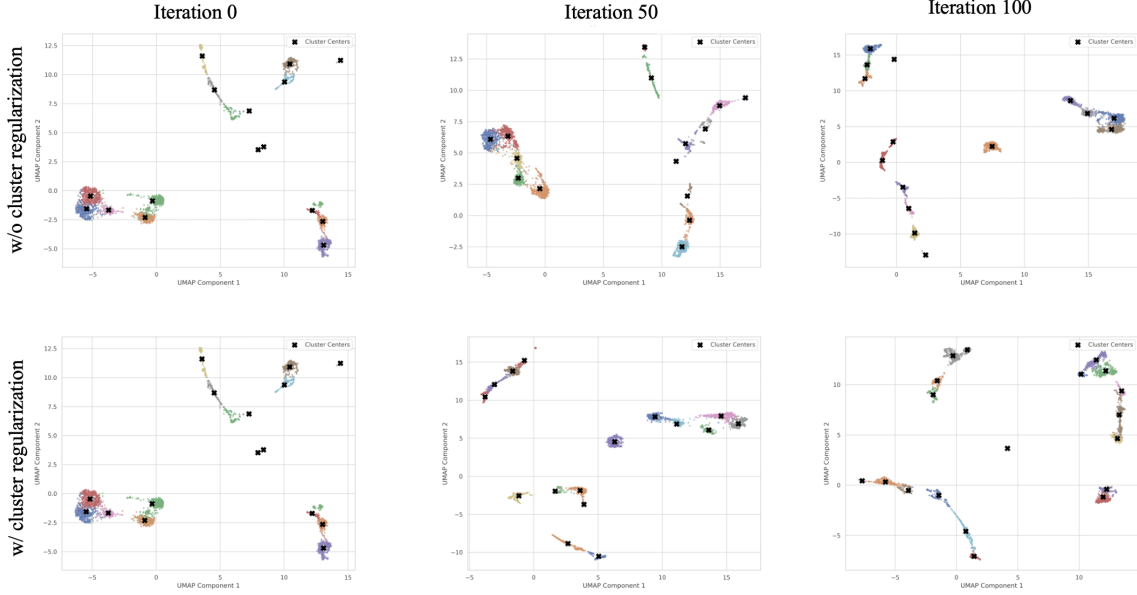


Fig. 5. UMAP visualizations showing clusters of different iterations during imputation. Better distinct clusters of UMAP plots helps with further analysis of single-cell data, such as the presence of rare cell types or intermediate states between well-defined populations.

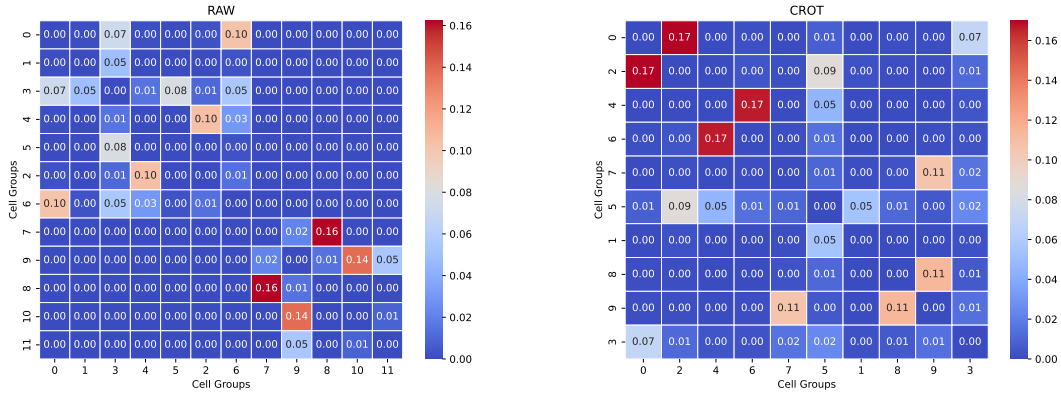


Fig. 6. PAGA similarity heatmap of RAW and imputed data.

DeepImpute⁵ We loaded two modalities of observed data as `data1`, `data2`, then initialized 5 JAMIE models with the epoch number in $\{300, 500, 700, 1000, 1500\}$, since the authors suggested 500 as their setting, and our data was larger. The other parameters were set as default. After training the initial model, we chose the best one and performed data imputation using observed entries.

AutoImpute⁶ Since AutoImpute utilizes `.csv` files, we first translated our data into `.csv` format. The key hyperparameter is `hidden_units`, which controls the size of the hidden layer or latent space dimensions, and we set `hidden_units=3500` instead of the default value of 2000.

scBFP⁷ We found `gene_k` and `cell_k = 40`, `gene_iter` and `cell_iter = 100`, provided the best performance.

DeepImpute⁸ We adjusted `limit` (Genes to impute, e.g., first 2000 genes. Default: `auto`) to equal the number of missing entries in each dataset, and conducted experiments under `max-epochs` in $\{300, 500, 700, 1000\}$. Our results showed that `max-epochs=700` performed best.

⁵ <https://github.com/lanagarmire/deepimpute>

⁶ <https://github.com/divyanshu-talwar/AutoImpute>

⁷ <https://github.com/Junseok0207/scBFP>

⁸ <https://github.com/lanagarmire/deepimpute>